Aust. J. Phys., 1974, **27**, 575–96

18 cm Observations of 19 New Southern OH Emission Sources

B. J. Robinson,[A] *J. L. Caswell*[A] *and W. M. Goss*[A,B]

[A] Division of Radiophysics, CSIRO, P.O. Box 76, Epping, N.S.W. 2121.
[B] Present address: Kapteyn Astronomical Institute, P.O. Box 800, Groningen 8002, The Netherlands.

Abstract

In a search for 1665 MHz OH emission in the southern Milky Way, 19 new sources have been discovered. Line profiles of all four 18 cm transitions are presented for all but one of the sources, and we discuss the general properties of the sources and their distribution in relation to the positions searched.

1. Introduction

Preliminary results of the present search for new OH emission sources at 1665 MHz have already been published (Robinson *et al.* 1971). The search was completed in May 1970 but subsequent observations have been made to obtain profiles in both senses of circular polarization for each of the four 18 cm transitions and to improve the position measurements.

The instrumentation and observing technique have been described by Robinson *et al.* (1970). The Parkes 64 m radio telescope was used with a 64-channel filter spectrometer: 10 kHz filter bandwidths were used in the initial search but the final detailed profiles were obtained with 1 kHz resolution. The telescope beamwidth to half-power is $12'\cdot2$ arc at 1665 MHz. The ratio of flux density to antenna temperature for an unpolarized point source is $1\cdot59\times10^{-26}$ W m^{-2} Hz^{-1} K^{-1}, for an assumed flux density of 36 f.u.* for the source Hydra A.

2. Results

In Table 1 we list the 19 OH sources together with the HII region nearest to each. One of these sources, OH $327\cdot3-0\cdot6$, was discovered during further inspection of the records and was not included in the preliminary report by Robinson *et al.* (1971). The positions of all sources have been redetermined with greater accuracy and the r.m.s. position errors are quoted. Column 7 shows the angular separation between the OH position and the continuum source peak. Column 8 shows the radial velocity separation of the OH source and the HII region in those cases where hydrogen recombination-line data are available for the continuum source. For completeness we have also listed in Table 1 the corresponding parameters for six other previously known OH sources (detected in earlier Parkes searches). These sources are discussed below in Section 4*c* in connection with the homogeneous search of the longitude range 255° to 350°. Improved positions and their r.m.s. errors are given for these sources also.

* 1 flux unit (f.u.) = 10^{-26} W m^{-2} Hz^{-1}.

Profiles for the 19 sources are given in Figs 1–19, and the dates of observation of each are given in Table 2. The filter bandwidth was 1 kHz for all profiles. Radial velocities are quoted relative to the local standard of rest. In Section 3 we discuss the relationship of the OH source to the nearest apparently associated HII region and any additional features of particular interest. In Section 4 we discuss the general properties of the sources as a group, including their distribution. Section 5 summarizes the new information and discusses it in the context of earlier work.

Table 1. 1665 MHz OH emission sources in the region 255° < *l* < 350°

(1) OH source number	(2) OH pos'n (1950) R.A. h m s s	(3) Dec. ° ′ ″ ″	(4) Nearest HII region	(5) HII pos'n (1950) R.A. h m s	(6) Dec. ° ′ ″	(7) Separation Position ′	(8) OH−HII Velocity* (km s^{-1})
			(a) New sources				
301·0+1·1	12 32 00·0±2·8	−61 22 39±20	G301·0+1·2	12 32 03	−61 22 42	0·4	6·9
308·9+0·1	13 39 37·0±2·4	−61 53 44±17	G309·1+0·2	13 40 39	−61 48 00	9·3	—
309·9+0·5	13 47 12·5±2·2	−61 19 58±16	G309·9+0·4	13 47 13	−61 25 00	5·0	—
320·2−0·3	15 06 00·3±3·1	−58 13 35±24	G320·3−0·3	15 06 18	−58 13 12	2·2	−0·2
324·2+0·1	15 29 01·8±2·7	−55 45 22±23	G324·2+0·1	15 29 02	−55 46 18	0·9	−5·0
327·3−0·6	15 49 12·8±4·0	−54 28 29±35	G327·3−0·6	15 49 11	−54 26 24	2·3	−20·2
328·2−0·5	15 54 04·9±2·7	−53 50 09±24	G328·2−0·6	15 54 14	−53 52 00	2·2	−1·7
330·9−0·4	16 06 29·8±2·2	−51 57 38±20	G330·9−0·4	16 06 26	−51 58 36	1·1	−7·4
330·9−0·2	16 06 05·0±1·7	−51 47 02±16	G331·0−0·2	16 06 21	−51 42 00	5·6	+3·2
331·4−0·3	16 08 35·8±3·2	−51 38 16±29	G331·3−0·3	16 08 32	−51 39 18	1·1	−2·6
337·7−0·1	16 34 49·8±1·7	−46 54 48±17	G337·6−0·0	16 34 31	−46 57 24	8·2	+5·0†
337·9−0·5	16 37 29·5±1·8	−47 02 02±18	G337·9−0·5	16 37 28	−47 01 36	0·4	−6·1‡
338·9−0·1	16 39 29·4±2·8	−46 03 05±29	G338·9−0·1	16 39 35	−46 00 48	2·6	+2·7
338·9+0·6	16 36 56·4±1·6	−45 35 53±17	G338·9+0·6	16 36 43	−45 34 24	3·0	+1·1
340·1−0·2	16 44 39·0±1·9	−45 16 26±20	G340·1−0·2	16 44 30	−45 15 18	1·9	−0·1
345·5+0·3	17 00 56·9±1·9	−40 39 38±21	G345·5+0·3	17 00 52	−40 42 00	2·6	—
345·7−0·1	17 03 22·8±1·3	−40 47 06±16	G345·6−0·0	17 02 41	−40 51 00	9·5	—
347·6+0·2	17 08 22·7±1·7	−39 05 09±20	G347·6+0·2	17 08 05	−39 05 00	3·4	+0·1
349·1+0·1	17 13 00·9±2·1	−37 56 06±25	G349·1−0·0	17 13 22	−37 58 00	4·6	−6·7
			(b) Previously known sources				
285·2−0·0	10 29 35·5±2·5	−57 46 27±20	G285·3−0·0	10 29 37	−57 46 42	0·4	+6
291·6−0·4	11 12 54·1±2·7	−60 53 08±20	G291·6−0·5	11 12 53	−60 59 24	6·3	+4
305·4+0·2	13 09 22·7±2·3	−62 21 15±16	G305·4+0·2	13 09 20	−62 18 48	2·4	+2
331·5−0·1	16 08 23·2±1·7	−51 20 45±16	G331·5−0·1	16 08 22	−51 19 24	1·3	−2
333·2−0·5	16 17 16·7±1·8	−50 27 45±17	G333·1−0·4	16 17 16	−50 29 12	1·4	+4
333·6−0·2	16 18 27·1±2·1	−49 59 01±20	G333·6−0·2	16 18 26	−49 58 54	0·6	−3

* HII region velocities are from the recombination-line measurements of Wilson *et al.* (1970) and Caswell (1972), except where otherwise noted. A dash indicates that no recombination-line data are available.
† A weaker HII region is closer to the OH position, and a previously unpublished H109α measurement at the OH position by one of us (J.L.C.) gave a velocity of −51 km s^{-1}, so that $V_{OH} - V_{HII} \approx +1$ km s^{-1}.
‡ The mean velocity of two OH features separated by 9 km s^{-1} is used.

3. Notes on Individual Sources

OH 301·0+1·1 (Fig. 1). The peak of the nearby continuum source G301·0+1·2 is less than 1′ arc away. It is a weak HII region (RCW 65) with a 5000 MHz flux density $S_{5000} \approx 3$ f.u. but of small angular size (~1′ arc), and thus is a compact HII region with high surface brightness (Shaver and Goss 1970*b*).

OH 308·9+0·1 (Fig. 2). The OH position lies between G309·1+0·2 (separation 9′ arc, $S_{2700} = 4$ f.u.) and G308·7+0·1 (separation 12′ arc, $S_{2700} = 12$ f.u.). The latter source is probably a supernova remnant (Clark *et al.* 1973) and the OH source is probably associated with the weak outlying portion of G309·1+0·2, which can be seen on the 2700 MHz map of Day *et al.* (1969).

OH309·9+0·5 (Fig. 3). The OH position is 5′ arc from G309·9+0·4 (S_{2700} = 5 f.u.) in the direction of G309·8−0·1 (S_{2700} = 8 f.u.). The map of Day *et al.* (1969) indicates the presence of emission between these peaks which requires further investigation with improved sensitivity and resolution.

OH320·2−0·3 (Fig. 4). The OH position is ∼2′ arc from the peak of G320·3−0·3, a thermal source with S_{5000} = 7·2 f.u. and angular size 2′·9 arc (Shaver and Goss 1970*b*).

OH324·2+0·1 (Fig. 5). The OH position is less than 1′ arc from G324·2+0·1, a thermal source with S_{5000} = 3·3 f.u. (Shaver and Goss 1970*b*). This HII region is of small diameter and is unresolved by the observations of Shaver and Goss. It is optically thick at 408 MHz and, in fact, possesses the third-highest turnover frequency amongst HII regions observed in their survey.

Table 2. Dates of observation of OH emission profiles

OH source	Fig. No.	Date of observation at indicated frequency (MHz) 1612	1665	1667	1720
301·0+1·1	1	18 July 1970	29 May 1970	30 May 1970[A] 25 Apr. 1971[A]	22 July 1970
308·9+0·1	2	18 July 1970	29 May 1970	30 May 1970	22 July 1970
309·9+0·5	3	18 July 1970	28 May 1970	25 May 1971	22 July 1970
320·2−0·3	4	13 June 1971	23 Apr. 1971	24 Apr. 1971	14 June 1971
324·2+0·1	5	13 June 1971	23 Apr. 1971	24 Apr. 1971	14 June 1971
327·3−0·6	6	—	5 May 1972	—	—
328·2−0·5	7	13 June 1971	2 Nov. 1970[B] 25 Apr. 1971[B]	2 Nov. 1970	14 June 1971
330·9−0·4	8	17 July 1970	29 May 1970	29 May 1970	21 July 1970
330·9−0·2	9	17 July 1970	28 May 1970	30 May 1970	21 July 1970
331·4−0·3	10	13 June 1971	23 Apr. 1971	24 Apr. 1971	14 June 1971
337·7−0·1	11	18 July 1970	28 May 1970	30 May 1970	21 July 1970
337·9−0·5	12	18 July 1970[C] 18 June 1971[C]	29 May 1970	25 Apr. 1971	21 July 1970[D] 14 June 1971[D]
338·9−0·1	13	13 June 1971	23 Apr. 1971	24 Apr. 1971	14 June 1971
338·9+0·6	14	18 July 1970	28 May 1970	24 Apr. 1971	21 July 1970
340·1−0·2	15	18 July 1970	29 May 1970	26 Apr. 1971	22 July 1970
345·5+0·3	16	19 July 1970	29 May 1970	30 May 1970	22 July 1970
345·7−0·1	17	14 June 1971	26 Apr. 1971	26 Apr. 1971	15 June 1971
347·6+0·2	18	14 June 1971	23 Apr. 1971	24 Apr. 1971	15 June 1971
349·1+0·1	19	18 July 1970	30 May 1970	26 Apr. 1971	22 July 1970

[A] LH, 25 Apr. 1971; RH, 30 May 1970.

[B] At V = −41·0 km s^{-1}, 2 Nov. 1970; at V = 37·4 km s^{-1}, 25 Apr. 1971.

[C] At V = −49·75 km s^{-1}, 18 July 1970; at V = −42·31 km s^{-1}, 18 June 1971.

[D] At V = −49·75 km s^{-1}, 21 July 1970; at V = −42·78 km s^{-1}, 14 June 1971.

OH327·3−0·6 (Fig. 6). The 1665 MHz emission in this direction was detected from a later inspection of the records and was not included in our initial list of 18 sources (Robinson *et al.* 1971). A 1 kHz resolution profile has been obtained only at 1665 MHz (Fig. 6). However, profiles with 10 kHz resolution obtained in our investigation of OH absorption in this direction (at V = −49 km s^{-1}) failed to detect any emission or absorption at 1667, 1612 or 1720 MHz near −70 km s^{-1} and thus the source is predominantly a 1665 MHz emitter. It is not clear whether the 1665 MHz emission is related to the main-line absorption feature near −49 km s^{-1}, which is accompanied by weak 1612 MHz satellite emission. The source G327·3−0·6 is an intense HII region with S_{5000} = 44·9 f.u. and angular size ∼1′ arc. It is optically thick at 408 MHz (Shaver and Goss 1970*b*) and its

peak is approximately 2′ arc from the OH position. Emission from H_2O has also been detected in this direction (Johnston *et al.* 1972) at a velocity of -60 km s^{-1}.

OH328·2−0·5 (Fig. 7). The OH position is ∼2′ arc from G328·2−0·6, which has $S_{2700} = 5$ f.u. (Day *et al.* 1969).

OH330·9−0·4 (Fig. 8). G330·9−0·4 is a small diameter (∼2′ arc) thermal source with $S_{5000} \approx 9$ f.u. (Shaver and Goss 1970*b*). Its peak is only 1′·1 arc from the OH position. The OH source has the strongest peak intensity at 1665 MHz of any source yet discovered: 498 f.u. in 1 kHz bandwidth, which is 12% stronger than W3 OH. Emission at 1612 MHz, although detected, is two orders of magnitude weaker than the main-line emission. Weak absorption is detectable at 1720 MHz, with peak optical depth of ∼0·06. The satellite-line features are best seen on profiles with 10 kHz resolution in Robinson *et al.* (1971).

OH330·9−0·2 (Fig. 9). The centre of G331·0−0·2 (or G331·0−0·1) is approximately 6′ arc from the OH position. However, the 5000 MHz map of Goss and Shaver (1970) shows a clear extension in the OH direction and the absence of this extension at 408 MHz (Shaver and Goss 1970*a*) suggests that a small-diameter HII region, which is optically thick at 408 MHz, is very near the OH position. Emission from H_2O has been detected in the direction of the OH emission (Johnston *et al.* 1972).

OH331·4−0·3 (Fig. 10). The OH position is 1′·1 arc from the peak of G331·3−0·3, an HII region with angular diameter of ∼3′ arc and $S_{5000} \approx 8$ f.u. (Shaver and Goss 1970*b*).

OH337·7−0·1 (Fig. 11). The OH position is approximately equidistant from the supernova remnant G337·8−0·1 (7′ arc) and the HII region G337·6−0·0 (8′ arc). Both continuum sources have widths to half-intensity of ∼5′ arc (Shaver and Goss 1970*b*). The HII region has $S_{5000} \approx 6$ f.u., while at 1666 MHz the supernova remnant has a flux density of ∼14 f.u. Absorption by OH is observed against the more intense source, the supernova remnant (Caswell and Robinson 1974, present issue pp. 597–627). Sensitivity greater than that of the present observations is needed to determine whether the OH absorbing cloud extends to cover the HII region.

It should also be noted that, on the 5000 MHz map (Goss and Shaver 1970), G337·6−0·0 shows a clear extension of the contours in the direction of the OH emission position, suggesting that a weak unresolved HII region (perhaps optically thick at 408 MHz) is very near the OH position.

OH337·9−0·5 (Fig. 12). The positions of OH features near both $V = -42$ and -52 km s^{-1} are the same to within 15″ arc and differ by less than 1′ arc from that of the peak of G337·9−0·5, a small-diameter (∼2′ arc) HII region which is optically thick at 408 MHz (Shaver and Goss 1970*b*) and which has $S_{5000} = 17$ f.u.

OH338·9−0·1 (Fig. 13). The HII region G338·9−0·1 is less than 3′ arc from the OH position. It is weak (3 or 4 f.u.) but of quite small diameter (∼2′ arc) and well separated from other sources (Shaver and Goss 1970*b*).

Figs 1–19 (pp. 579–88). Profiles of OH emission for the indicated sources showing RH (full curves) and LH (dashed curves) circular polarization. The filter bandwidths are 1 kHz and the radial velocities are given relative to the local standard of rest.

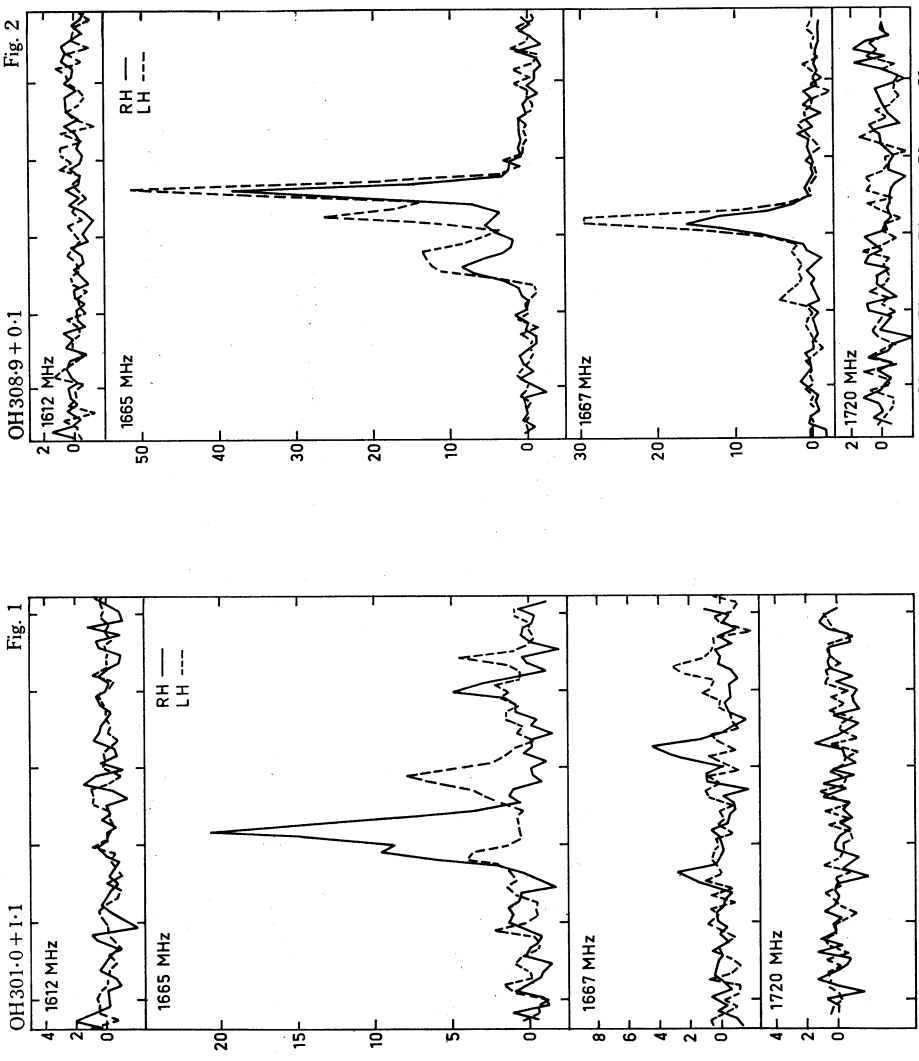
Fig. 1
OH301·0+1·1
1612 MHz
1665 MHz
1667 MHz
1720 MHz
RH
LH
Antenna temperature (K)
V_{lsr} (km s^{-1})

Fig. 2
OH308·9+0·1
1612 MHz
1665 MHz
1667 MHz
1720 MHz
RH
LH
V_{lsr} (km s^{-1})

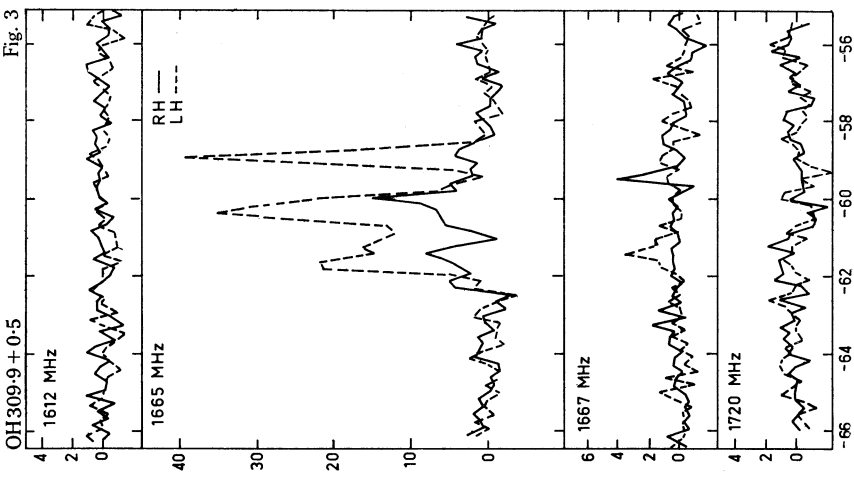
OH309·9+0·5
1612 MHz
1665 MHz
RH
LH
1667 MHz
1720 MHz
Antenna temperature (K)
V_{lsr} (km s^{-1})

Fig. 3

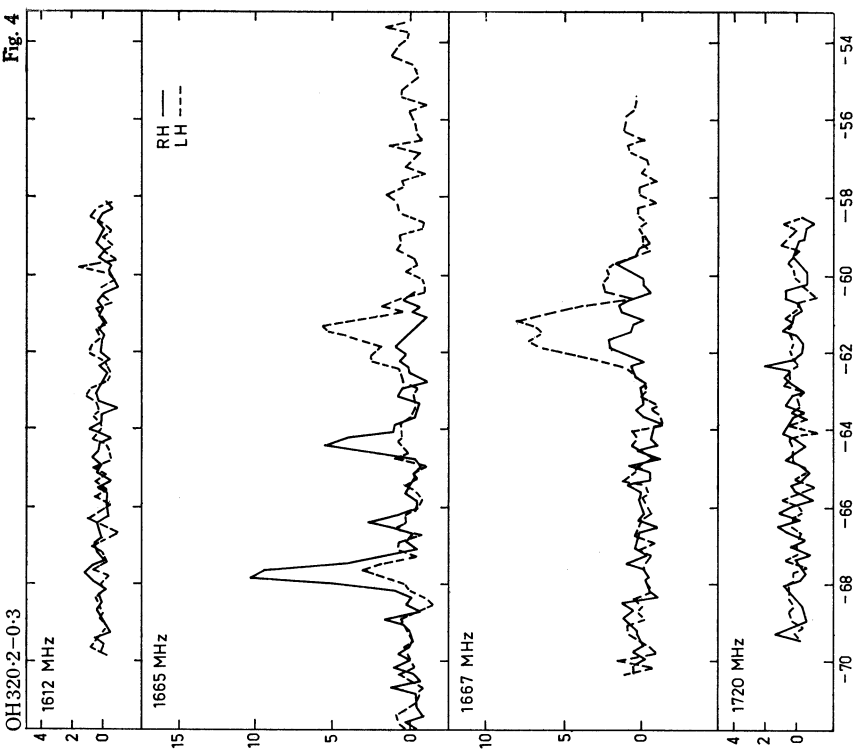
OH320·2−0·3
1612 MHz
1665 MHz
RH
LH
1667 MHz
1720 MHz
V_{lsr} (km s^{-1})

Fig. 4

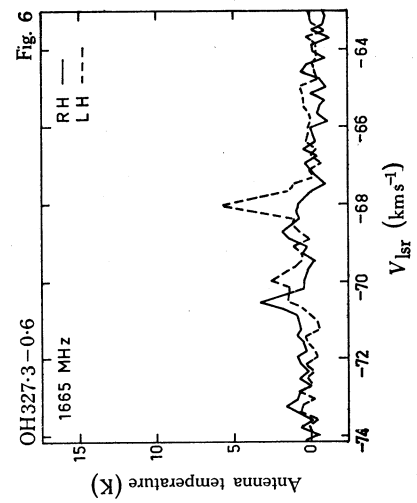
Fig. 6
OH327·3−0·6
1665 MHz
RH —
LH ---
Antenna temperature (K)
V_{lsr} (km s^{-1})

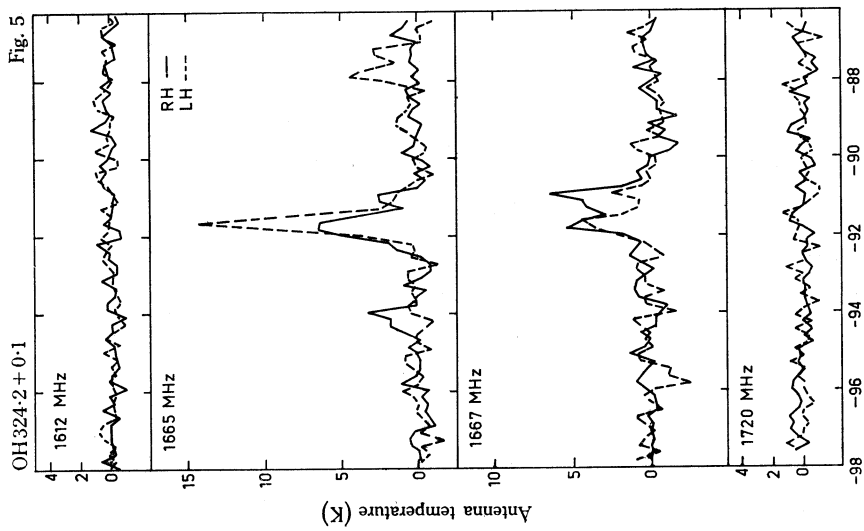
Fig. 5
OH324·2+0·1
1612 MHz
1665 MHz
1667 MHz
1720 MHz
RH —
LH ---
Antenna temperature (K)
V_{lsr} (km s^{-1})

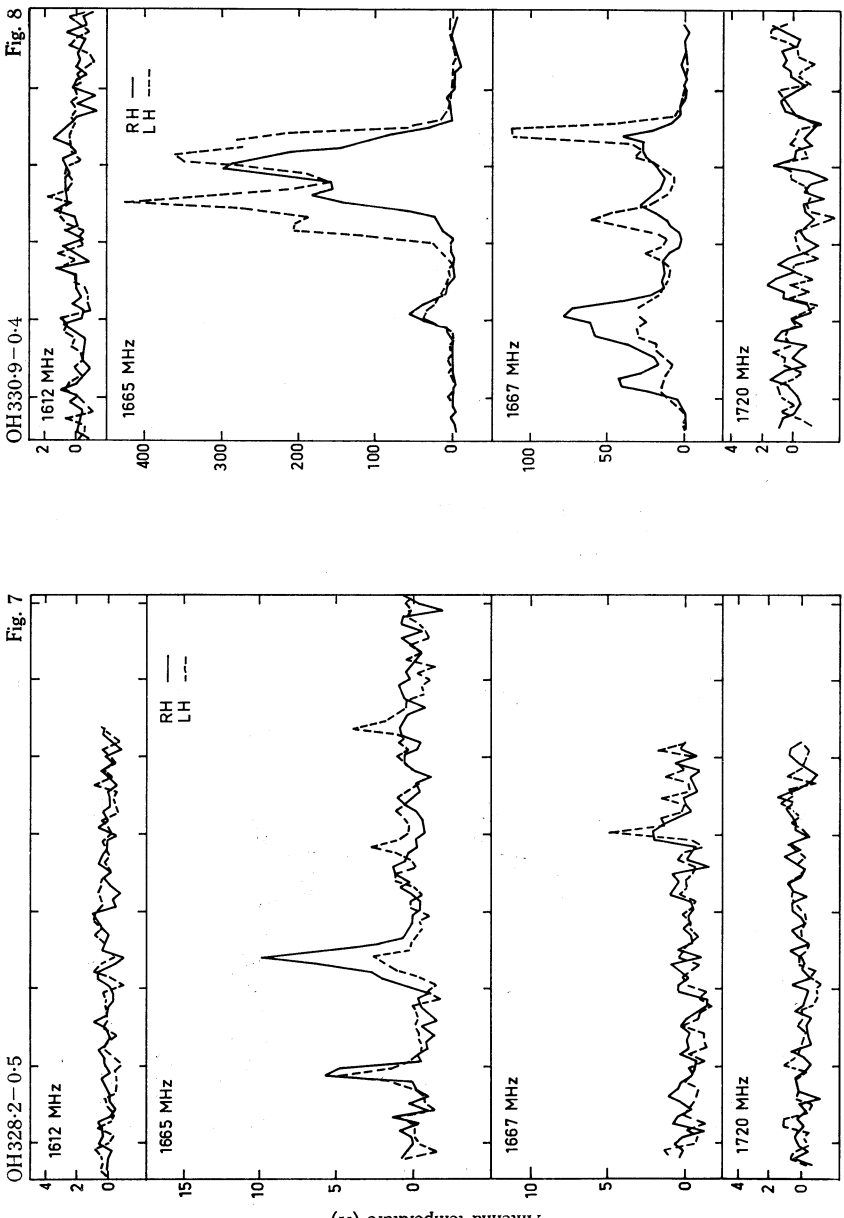
OH330·9−0·4
1612 MHz
1665 MHz
1667 MHz
1720 MHz
RH
LH
V_{lsr} (km s^{-1})

Fig. 8

OH328·2−0·5
1612 MHz
1665 MHz
1667 MHz
1720 MHz
RH
LH
Antenna temperature (K)
V_{lsr} (km s^{-1})

Fig. 7

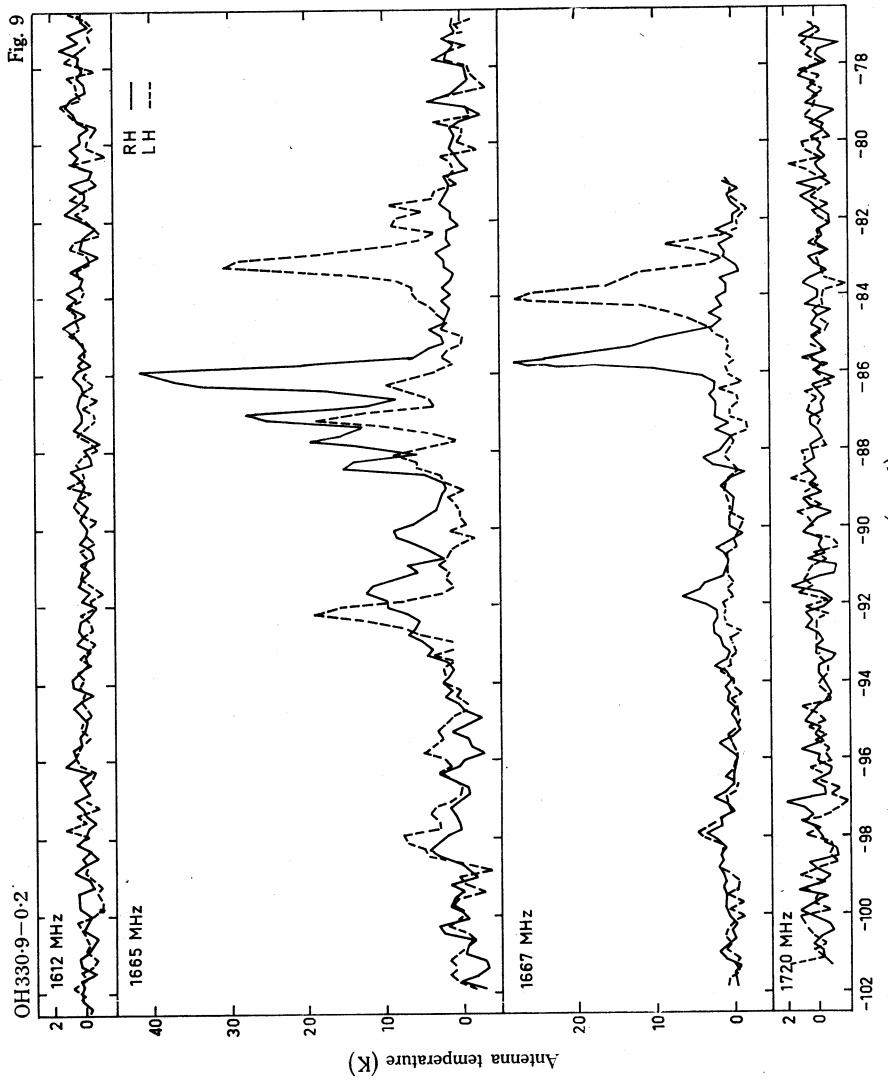
OH330·9−0·2
1612 MHz
1665 MHz
1667 MHz
1720 MHz
RH
LH
Antenna temperature (K)
V_{lsr} (km s^{-1})

Fig. 9

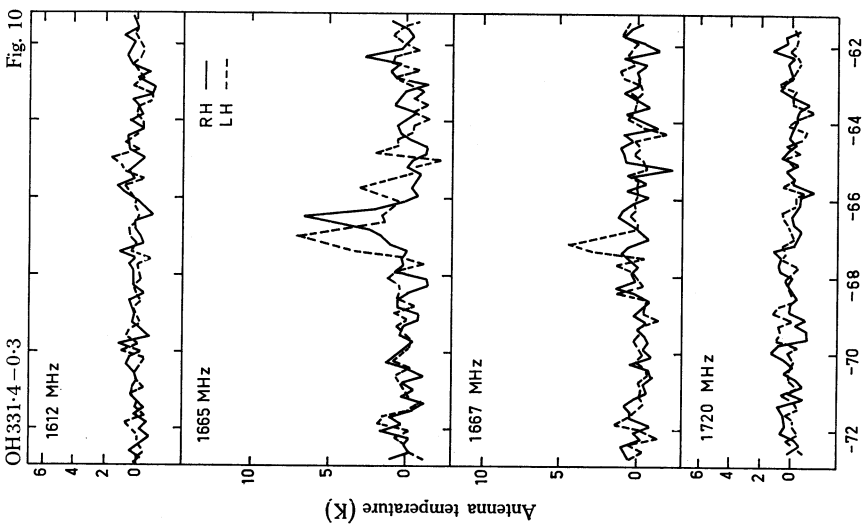
OH331·4−0·3
1612 MHz
1665 MHz
1667 MHz
1720 MHz
RH
LH
Antenna temperature (K)
V_{lsr} (km s^{-1})

Fig. 10

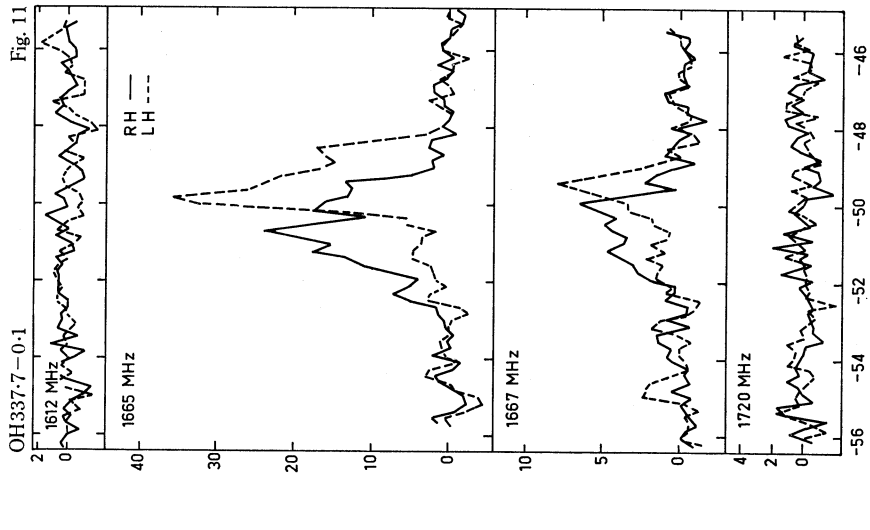
OH337·7−0·1
1612 MHz
1665 MHz
1667 MHz
1720 MHz
RH
LH
V_{lsr} (km s^{-1})

Fig. 11

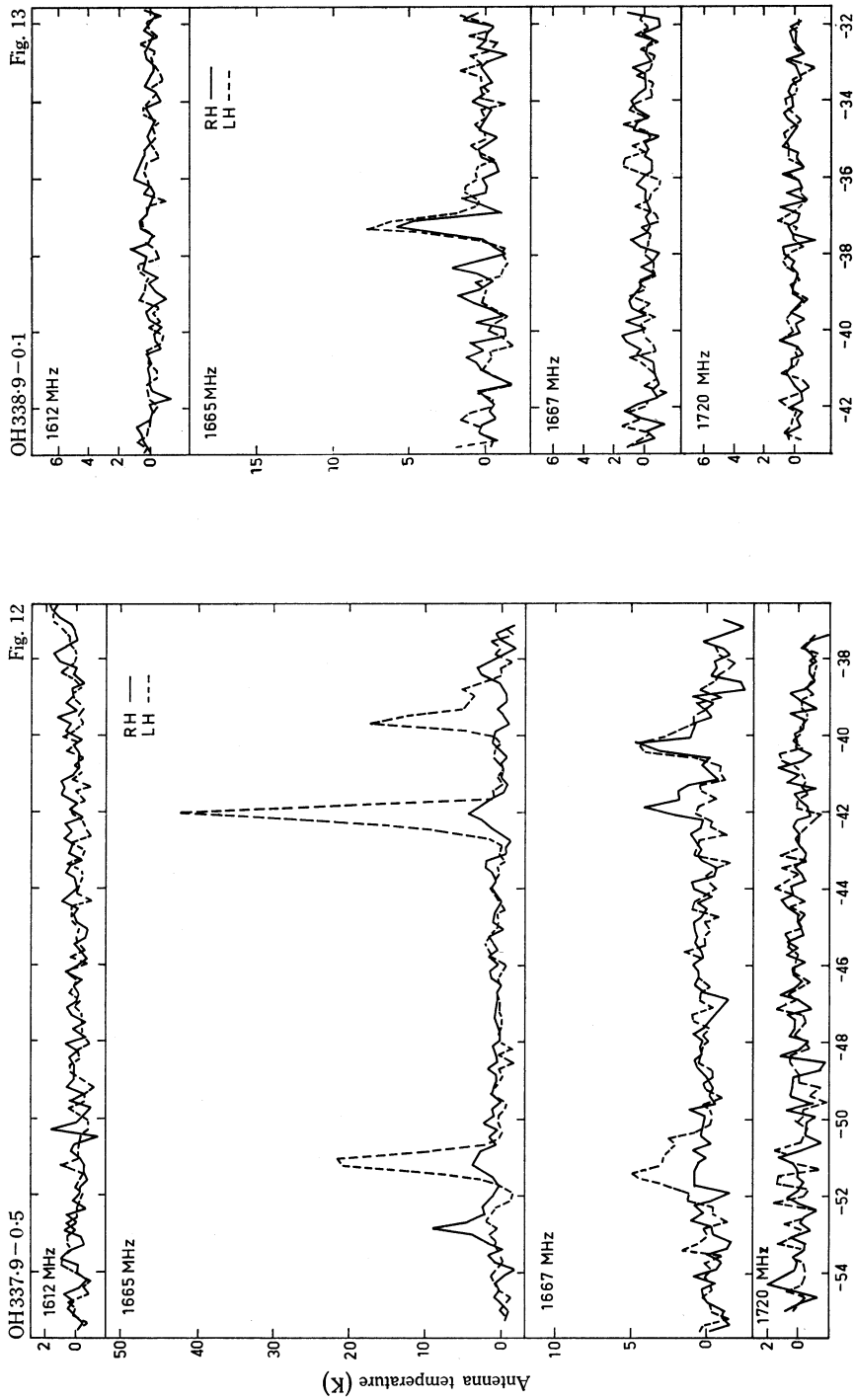
Fig. 13
OH338·9−0·1
1612 MHz
1665 MHz
1667 MHz
1720 MHz
RH
LH
V_{lsr} (km s^{-1})

Fig. 12
OH337·9−0·5
1612 MHz
1665 MHz
1667 MHz
1720 MHz
RH
LH
Antenna temperature (K)
V_{lsr} (km s^{-1})

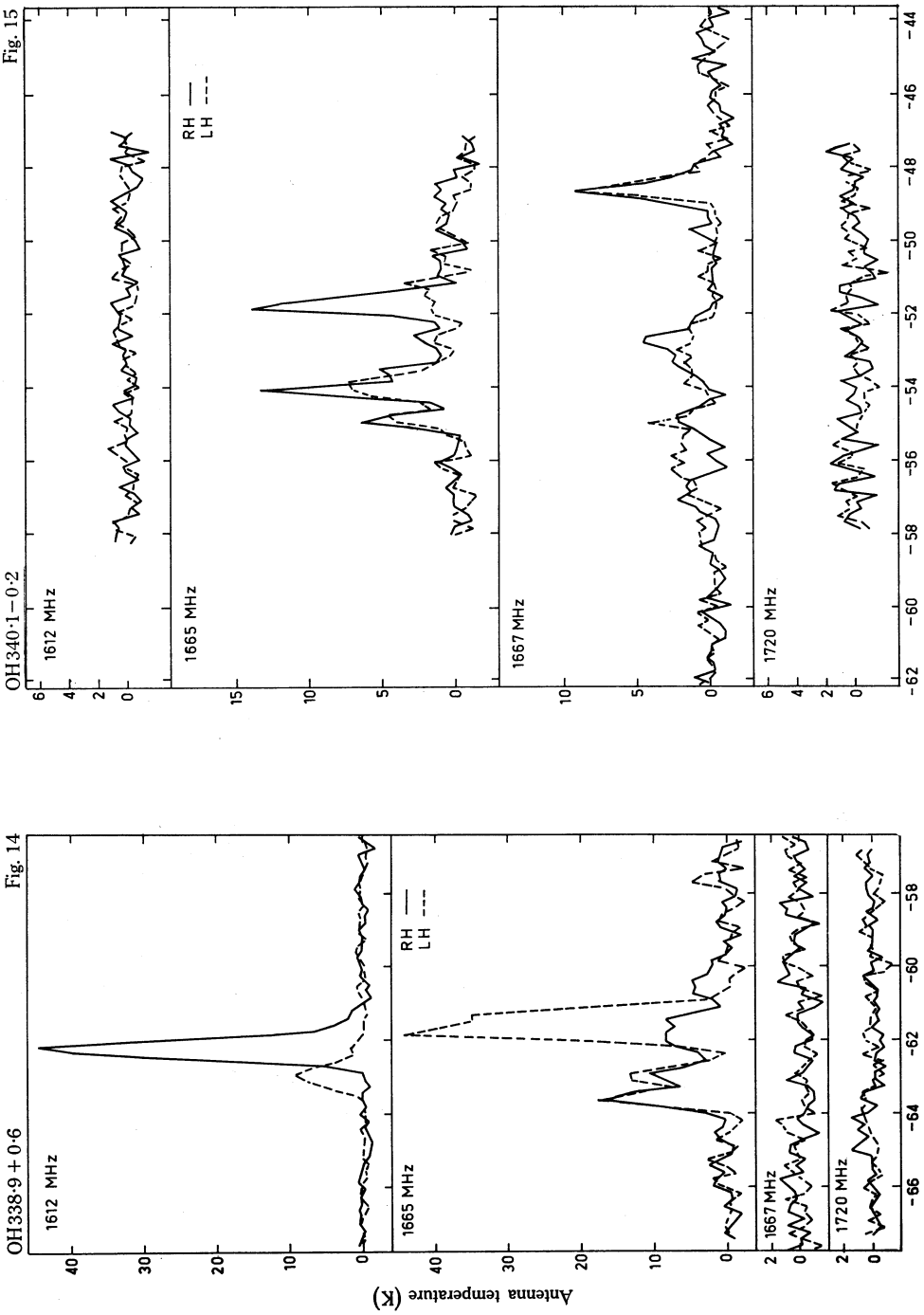
OH338·9 + 0·6
1612 MHz
1665 MHz
RH
LH
1667 MHz
1720 MHz
Antenna temperature (K)
V_{lsr} (km s^{-1})

Fig. 14

OH340·1−0·2
1612 MHz
1665 MHz
RH
LH
1667 MHz
1720 MHz
V_{lsr} (km s^{-1})

Fig. 15

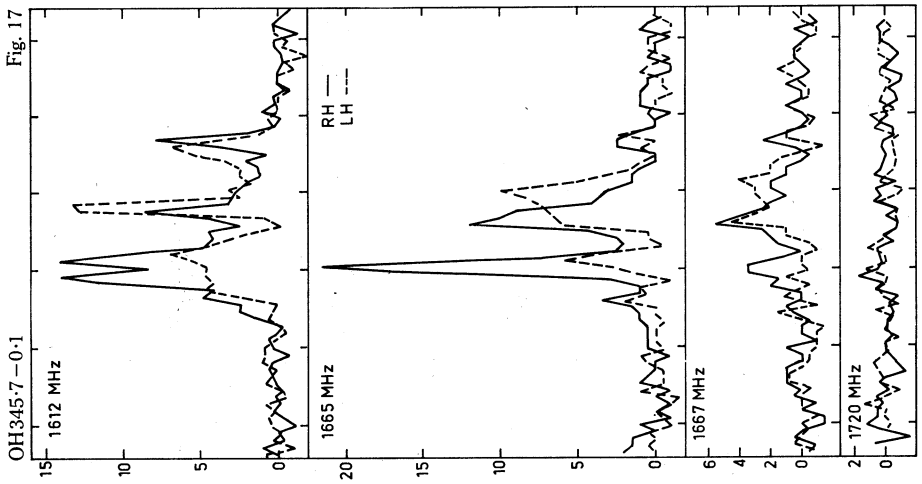
OH345·7−0·1
1612 MHz
1665 MHz
1667 MHz
1720 MHz
RH —
LH ---
V_{lsr} (km s^{-1})

Fig. 17

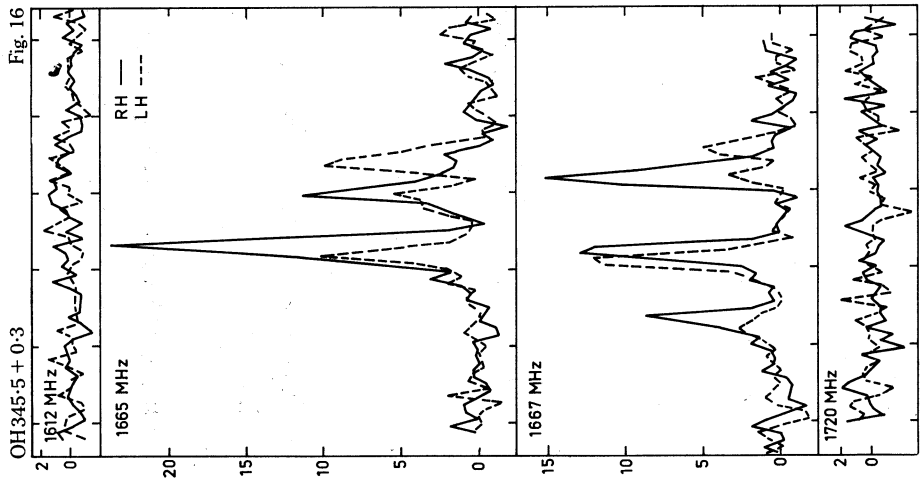
OH345·5 + 0·3
1612 MHz
1665 MHz
1667 MHz
1720 MHz
RH —
LH ---
Antenna temperature (K)
V_{lsr} (km s^{-1})

Fig. 16

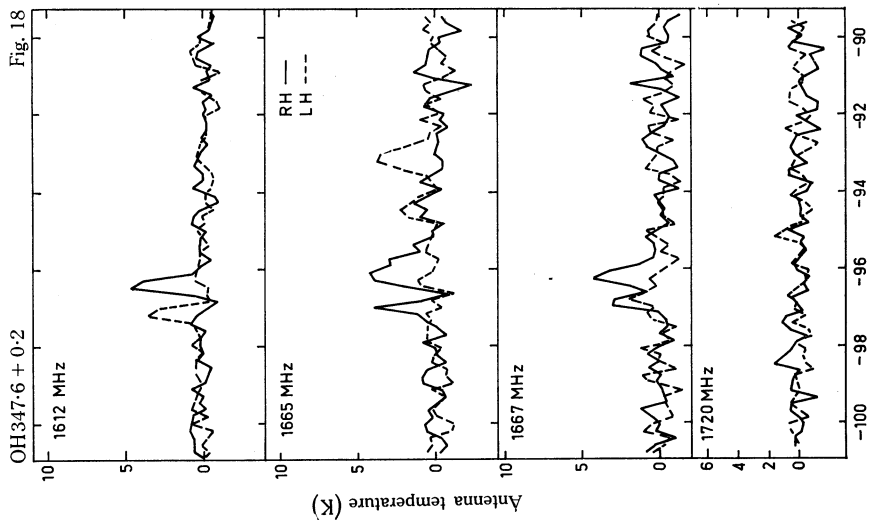
OH347·6 + 0·2
Fig. 18
1612 MHz
1665 MHz
RH —
LH ---
1667 MHz
1720 MHz
Antenna temperature (K)
V_{lsr} (km s^{-1})

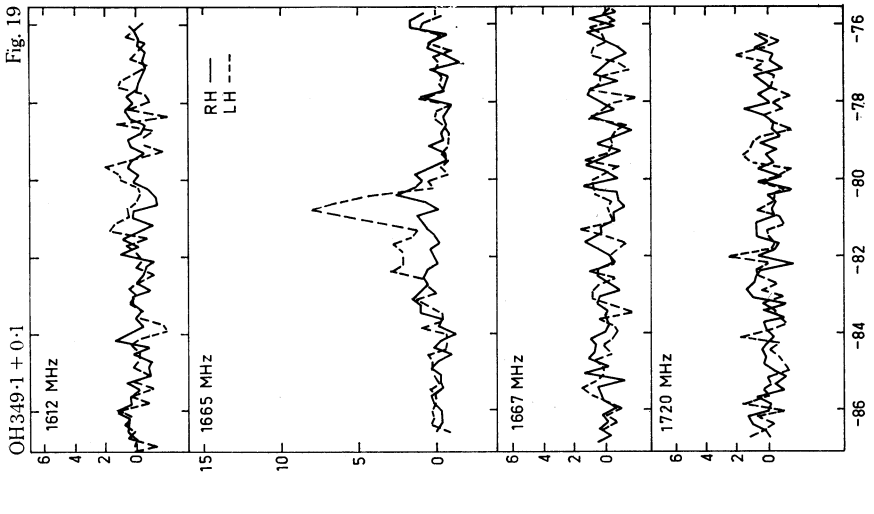
OH349·1 + 0·1
Fig. 19
1612 MHz
1665 MHz
RH —
LH ---
1667 MHz
1720 MHz
V_{lsr} (km s^{-1})

OH338·9+0·6 (Fig. 14). The HII region G338·9+0·6 (Shaver and Goss 1970*b*) has $S_{5000} \approx 10$ f.u. and an angular size of 3′·5 arc, with its peak ~3′ arc from the OH position. The OH characteristics are unusual in that 1667 MHz emission is not detectable, whereas 1612 MHz emission is present with an intensity comparable with that at 1665 MHz. Features of weak emission at 1720 MHz and weak absorption at 1667 MHz are quite broad in velocity and more readily seen after smoothing to a lower frequency-resolution. The peak optical depth at 1667 MHz is ~0·08.

OH340·1−0·2 (Fig. 15). A weak HII region G340·1−0·2 is ~2′ arc from the OH position. From the 5000 MHz map of Goss and Shaver (1970) we estimate its intensity to be 4 f.u. with maximum possible error of 2 f.u.

OH345·5+0·3 (Fig. 16). The highest resolution map available is at 2700 MHz (Beard *et al.* 1969). The source G345·5+0·3 has $S_{2700} \approx 4$ f.u., width to half-intensity of 3′ arc, and is less than 3′ arc from the OH position.

OH345·7−0·1 (Fig. 17). The 1665 MHz OH emission is accompanied by weaker 1612 MHz emission and even weaker 1667 MHz emission. The highest resolution map available, that at 2700 MHz (Beard *et al.* 1969), shows G345·6−0·0 to be the nearest continuum source. It has $S_{2700} = 28$ f.u. and it is extended (10′ × 6′ arc), with the peak separated by nearly 10′ arc from the OH position. Higher resolution and sensitivity are desirable to determine whether any small HII components are more closely associated with the OH position. Emission from H_2O has been detected (Johnston *et al.* 1972) coincident with the OH.

OH347·6+0·2 (Fig. 18). The intensities of OH emission at 1665, 1667, and 1612 MHz are comparable. The 2700 MHz continuum map (Beard *et al.* 1969) shows that G347·6+0·2 is within ~3′ arc of the OH position. It has $S_{2700} = 22$ f.u. and its angular size is 7′ × 3′ arc.

OH349·1+0·1 (Fig. 19). The 2700 MHz map (Beard *et al.* 1969) shows G349·1−0·0 to be the nearest continuum source (separation 4′·6 arc). It has an angular size of 6′ arc and $S_{2700} = 12$ f.u.

4. Discussion

(*a*) *Intensity ratios of the four 18 cm transitions*

The 19 sources all belong to a class of main-line emitters believed to be physically associated with HII regions. None of the sources shows emission significantly stronger on any line other than the 1665 MHz line (at which it was discovered). None shows detectable 1720 MHz emission, only 3 of the 19 show 1612 MHz emission and 15 show 1667 MHz emission. A complementary search at 1667 MHz (Caswell and Robinson 1974, present issue pp. 597–627) which covered over half the stronger continuum sources searched at 1665 MHz (primarily to detect new absorption features) failed to find any sources of 1667 MHz emission additional to those already discovered at 1665 MHz and listed in Table 1 above. Turner's (1970) northern search, made at 1665 and 1667 MHz simultaneously, also supports the conclusion that in the direction of HII regions it is most unusual for 1667 MHz emission not to be accompanied by somewhat stronger 1665 MHz emission.

Table 3. Galactic continuum sources searched for 1665 MHz OH emission

(1) Source	(2) V_0 (km s^{-1})	(3) S_{2700} (f.u.)	(4) Notes	(1) Source	(2) V_0 (km s^{-1})	(3) S_{2700} (f.u.)	(4) Notes
G256·6+0·6	+10	2		G299·0+0·2	0	4	
G261·4+0·9	+10	5		G301·0+1·2	−30	3	OH 301·0+1·1
G262·0−0·5	+10	1		G301·1+1·0	−30	4	
G264·3+1·5	+10	3		G301·9+1·1	−30	<3	
G265·1+1·5	+10	22		G302·5−0·8	−30	<3	
G267·9−1·0	+10	185		G302·7+0·2	−30	<3	
G268·4−0·8	+10	5		G303·5−0·6	−30	2	Footnote [B]
G269·1−1·1	+10	7		G304·6+0·1	0	8	Probable SNR
G269·2−1·4	+10	12		G305·2−0·4	0	6	
G269·4−1·5	+10	2		G305·2+0·0	+5	102	
G270·4−1·0	+10	4		G305·3+0·2	−35	122	OH 305·4+0·2
G270·3+0·9	−5	4		G305·6+0·0	+5	29	
G274·0−1·1	−5	28		G305·7+1·6	−30	⩾3	
G281·0−1·5	0	8		G306·2+0·1	−30	<3	
G282·0−1·2	0	36		G306·3−0·3	−30	<3	
G282·6−0·8	0	3		G307·6−0·3	+5	12	
G283·3−0·6	0	10		G308·7+0·1	+5	12	Probable SNR
G283·5−1·0	0	8		G308·7+0·6	+5	21	
G284·0−0·9	0	81	Footnote [A]	G308·8−0·2	−30	4	
G284·2−1·8	0	13		G309·1+0·2	−30	4	OH 308·9+0·1
G284·3+0·4	0	6		G309·2−0·4	−30	3	
G284·3−0·3	0	152		G309·5−0·7	−30	3	
G284·7+0·3	0	4		G309·8−0·1	+5	8	SNR
G285·0−2·0	0	3		G309·9+0·4	−50	5	OH 309·9+0·5
G285·3−0·0	0	18	OH 285·2−0·0	G310·2−0·1	−50	6	
G285·5−0·0	0	4		G310·5+0·2	−30	4	
G285·8+0·1	0	1		G310·7−0·3	−50	5	
G286·0−1·1	0	3		G310·9−0·4	−50	8	
G286·2−0·2	0	35		G311·0+0·4	−30	4	
G286·4−1·4	0	7		G311·1−0·3	−25	3	
G287·1−2·1	0	3		G311·3+0·1	−50	7	
G287·3−2·2	0	2		G311·5+0·4	−50	10	
G287·3+0·4	0	4		G311·5−0·4	−50	6	
G289·1−0·4	0	14		G311·6−0·6	−25	3	
G289·8−1·1	0	43		G311·9+0·1	−50	28	
G289·9−0·8	−5	5		G312·3−0·3	−50	10	
G290·1−0·8	−5	20	Probable SNR	G312·6+0·2	−25	3	
G290·5−0·8	0	4		G313·5+0·2	−50	6	
G290·6+0·3	0	4		G314·2+0·4	−50	11	
G290·8+0·8	0	3		G315·3−0·2	−50	5	SNR
G291·0−0·1	−5	15	Probable SNR	G316·3−0·0	−50	12	Probable SNR
G291·1−0·8	−5	>3		G316·4−0·4	−50	5	
G291·2−0·3	−5	5		G316·8−0·0	−45	34	
G291·3−0·7	0	95		G317·0+0·3	−45	17	
G291·5−0·1	0	4		G317·3+0·3	−45	12	
G291·6−0·5	0	238	OH 291·6−0·4	G317·6−0·4	−50	4	
G291·8−0·7	0	3		G317·8+0·2	−50	3	
G291·9−1·0	0	6		G318·0−0·7	−50	7	
G292·0+1·8	0	10	Probable SNR	G318·1−0·4	−50	4	
G293·6−1·3	0	5		G318·2−0·6	−50	6	
G294·8−1·7	0	9		G318·3+0·1	−50	3	
G295·0−1·7	0	12		G318·9−0·1	−50	3	
G295·2−0·6	0	20		G319·0+0·4	−50	5	
G296·6−1·0	0	3		G319·2−0·3	−50	19	
G296·8−0·3	0	4	SNR	G319·3+1·1	−50	1	
G297·5−0·8	0	4		G319·4+0·0	−50	12	
G298·2−0·8	0	3		G319·9+0·8	−50	2	
G298·2−0·3	0	40		G320·1−0·5	−50	2	
G298·6−0·1	0	13		G320·2+0·8	−50	10	
G298·9−0·4	0	52		G320·3−0·2	−50	12	

[A] OH 284·2−0·8, though discovered while searching this position (Manchester *et al.* 1970), is probably an unrelated object of the OH/IR type.

[B] Search position was at 303·45−0·7, between two weak sources.

Table 3 (*Continued*)

(1) Source	(2) V_0 (km s^{-1})	(3) S_{2700} (f.u.)	(4) Notes	(1) Source	(2) V_0 (km s^{-1})	(3) S_{2700} (f.u.)	(4) Notes
G320·3−0·3	−50	9	OH 320·2−0·3	G332·8−1·4	−50	<3	
G320·3+0·4	−50	2		G334·7−0·2	−50	<3	
G320·3−1·0	−50	23	Part of SNR	G334·9−0·3	−50	<3	
G320·3−1·4	−50	12	Part of SNR	G335·1+0·1	−50	<3	SNR
G320·4+0·2	−50	5		G335·7+0·1	−50	<3	
G320·7+0·2	−50	9		G335·8−0·1	−50	10	
G321·1−0·5	−50	21		G336·0+0·1	−50	4	
G321·5+1·0	−50	1		G336·3+0·3	−45	<3	
G321·6−0·7	−50	2		G336·4−0·0	−45	<3	
G321·6−1·9	−50	1		G336·4−0·2	−45	35	
G321·7+1·2	−50	2		G336·5−1·5	−45	6	
G321·8−0·2	−50	1	SNR	G336·7+0·5	−45	<3	Probable SNR
G322·1+1·5	−50	3		G336·8+0·0	−45	70	
G322·2+0·6	−50	14		G337·1−0·2	−45	30	
G322·3−1·2	−50	2	Nonthermal	G337·2−0·7	−45	<3	SNR
G322·5−0·1	−50	<1		G337·3+1·0	−45	5	SNR
G322·5+0·2	−50	1		G337·8−0·1	−45	35	OH 337·7−0·1
G322·7−0·3	−50	1		G337·9−0·5	−45	16	OH 337·9−0·5
G323·5+0·1	−50	4	Partly SNR	G338·0−0·1	−45	50	
G323·5−0·2	−50	1		G338·4−0·2	−45	<3	
G323·9+0·0	−50	1		G338·4+0·1	−45	95	
G324·1−0·9	−45	3		G338·9+0·6	−45	11	OH 338·9+0·6
G324·2+0·2	−45	10	OH 324·2+0·1	G338·9−0·1	−45	3	OH 338·9−0·1
G324·9−0·5	−45	5		G339·1−0·4	−50	4	
G325·3−0·1	−45	2		G339·3+0·2	−45	3	
G325·3+0·4	−45	1		G339·8+0·3	−45	3	
G325·6+1·7	−45	1		G340·1−0·2	−50	5	OH 340·1−0·2
G326·2−1·7	−45	91	Probable SNR	G340·2+0·5	−45	4	
G326·3+0·7	−45	14		G340·3−0·2	−50	9	
G326·4+0·9	−45	16		G340·8−1·0	−50	18	
G326·6−0·5	−45	18		G341·1−0·1	−50	6	
G326·7+0·6	−45	50		G341·2−0·3	−50	5	
G326·9−0·0	−45	20		G341·9−0·3	−45	<3	
G327·2−1·1	−45	4	SNR	G342·0+0·4	−45	3	
G327·3+0·4	−45	12	SNR	G342·3+0·3	−50	6	
G327·3−0·5	−45	54	OH 327·3−0·6	G342·4−0·0	−45	3	
G327·4+1·1	−45	1		G342·3−0·5	−45	4	
G327·6−0·4	−45	9		G343·5−0·0	−45	15	
G327·8+0·1	−50	12		G344·9+1·7	−55	13	
G328·0−0·1	−50	8		G345·0+1·5	−55	>3	
G328·2−0·6	−50	5	OH 328·2−0·5	G345·2+1·0	−55	18	
G328·3+0·4	−50	8		G345·2−0·8	−55	10	
G328·4+0·2	−50	11	Probable SNR	G345·4+1·4	−50	30	
G328·6−0·5	−50	9		G345·4−0·9	−40, −55	33	
G331·4+1·0	−50	6	Footnote [C]	G345·5+0·3	−40	4	OH 345·5+0·3
G331·4+0·5	−50	<2	Footnote [D]	G345·6−0·0	−55	28	OH 345·7−0·1
G331·0−0·2	−50	15	OH 330·9−0·2	G346·2−0·1	−55	9	
G330·8−0·4	−50	22	OH 330·9−0·4	G346·6−0·2	−40	2·5	SNR
G331·1−0·5	−50	10	Footnote [E]	G347·6+0·2	−50	22	OH 347·6+0·2
G331·5−0·1	−50	47	OH 331·5−0·1	G348·2−1·0	−50	10	
G331·3−0·3	−50	17	OH 331·4−0·3	G348·2+0·5	−50	7·5	
G333·0+0·8	−50	5		G348·5+0·1	−50	45	Nonthermal
G332·5+0·1	−50	4	Probable SNR	G348·6−0·6	−50	15	
G332·1−0·4	−50	12		G348·7−1·0	−50	62	
G332·4−0·4	−50	15	SNR	G348·7+0·3	−30	21	Nonthermal
G333·2−0·1	−50	4		G349·1−0·0	−50	12	OH 349·1+0·1
G332·7−0·6	−50	52		G349·5+1·0	−40	3	
G333·1−0·5	−50	52	OH 333·2−0·5	G349·7+0·2	−40	13	Nonthermal
G333·3−0·4	−50	60		G349·8−0·6	−40	7·5	
G333·6−0·2	−50	122	OH 333·6−0·2	G351·7−1·2	−35	43	

[C] Not covered by 2700 MHz maps; continuum flux density from unpublished data of one of us (J.L.C.).

[D] Search position was 5′ arc south of continuum source.

[E] Note that Beard's (1966) declination of −49°53′·1 should be corrected to −51°53′·1.

(*b*) *Polarization and velocity structure*

The profiles (Figs 1–19) reveal that all emission features are in general strongly circularly polarized and that emission is present at a number of different velocities. Features observed on different transitions do not show any detailed correspondence in velocity or intensity. Single features are often 100% circularly polarized and, where an apparently single feature is detectable in both senses of polarization of a transition, there are usually small differences in the velocity and shape of the feature for the two polarizations. In such cases it is probable that we are observing the juxtaposition of two sources each with $\sim 100\%$ polarization. We have thus not attempted to tabulate the polarization properties since this would necessarily oversimplify them. When features are more than 2 or 3 kHz wide, the shape is complex and the polarization usually varies across the profile, suggesting that we are observing blends of several features whose separation is somewhat less than their intrinsic widths. There is little prospect of reliably separating these except by interferometry, on the basis of the very small positional differences expected ($\lesssim 1''$ arc). On profiles where at least two intense features are present, we have confirmed that any positional separations are within the positional errors (in a number of cases less than 15″ arc). In the case of OH 337·9−0·5, for example, two quite distinct features separated by 9 km s^{-1} in velocity have the same position to within less than 15″ arc.

Four of the present sources have also been observed by Dickinson and Turner (1972), who tabulated polarization values for the main lines but published no profiles. We note the following discrepancies:

(1) Dickinson and Turner listed 349·15+0·0 at $V = -80{\cdot}9$ km s^{-1} (source OH 349·1+0·1 in the present list) as $100 \pm 14\%$ RH circularly polarized. Our observations showed 100% LH (30 May 1970), and additional observations in May 1972 also gave the same LH intensity, suggesting that the Dickinson and Turner sense of polarization is in error.*

(2) For OH 337·7−0·1, 345·7−0·1 and 347·6+0·2, Dickinson and Turner quoted low values of polarization which appear to be averages over several features. Our high-resolution profiles show that individual features are highly polarized but in opposite senses.

(*c*) *Distribution of sources*

(i) *Region Searched*

Table 3 lists all the galactic continuum sources which we searched for 1665 MHz OH emission in the range $255° < l < 352°$. Their equatorial coordinates can be found in the Parkes 2700 MHz galactic surveys (Beard 1966; Beard *et al.* 1969; Day *et al.* 1969; Thomas and Day 1969*a*; Thomas and Day 1969*b*; Day *et al.* 1972). The radial velocities searched in each case covered a 100 km s^{-1} range centred on the value V_0 listed in column 2 (quoted to the nearest 5 km s^{-1}). We have added to the list the six 1665 MHz emission sources previously detected in this region (Goss *et al.* 1970; Manchester *et al.* 1970) for which positions are given in Table 1. The null results of earlier searches were rechecked in the present search, and thus Table 3 summarizes an effectively homogeneous search of the longitude range 255° to 350°.

* In defining the sense of circular polarization we follow the radio convention, by which RH polarized means RH about the direction of propagation.

The search list covers discrete sources with flux density at 2700 MHz greater than 3 f.u. and consists mainly of HII regions. However, it does include a number of supernova remnants (Milne 1970; Shaver and Goss 1970*b*; Clark *et al.* 1973) noted as 'SNR' or 'nonthermal' in column 4 of Table 3. No OH in emission was found at these positions and so these sources are not included in the statistics of the HII regions searched. We also searched some sources weaker than 3 f.u., again with no positive results, and these too are omitted from the statistics of the HII region search. Finally, some regions specifically excluded from the search are: the Vela and Puppis supernova remnants, the Carina nebula, some weak features within the complex RCW 46+48+49+50, and a few sources near the 3 f.u. limit not present in the preliminary versions of 2700 MHz source lists available at the time of the search.

During the search the $12' \cdot 2$ arc beam of the 64 m telescope was directed at the continuum maximum of each source. The OH sensitivity limits were as described by Robinson *et al.* (1971). In column 4 of Table 3, sources in which 1665 MHz emission was discovered are indicated by an OH source number.

(ii) *Association of 1665 MHz OH with HII Regions*

Most surveys for 1665 MHz OH emission have selected HII regions as the initial search positions. There is a risk that this selection would bias the apparent correlation of 1665 MHz emission with discrete HII regions. The only unbiased search is that by Ellder *et al.* (1969), who surveyed an area in Cygnus. They detected three sources of 1665 MHz emission which agree closely in position with compact components of HII regions. In the case of ON-1, however, the continuum source is extremely weak and was only found after a high-sensitivity search at the OH position (Winnberg *et al.* 1973).

In the present survey the OH sources were found at positions displaced from the maxima of the continuum sources searched. Where the continuum radiation has been surveyed with adequate sensitivity and resolution there usually appears to be a small-diameter HII region associated with the OH emission. In many cases the HII region is sufficiently compact to be optically thick at 408 MHz. Where H109α recombination-line observations are available, the OH almost always lies in the velocity range between the half-intensity points of the recombination line (see Table 1). The velocity width of the H109α line is typically greater than ± 10 km s^{-1} to half-intensity, and much of this broadening is the result of turbulent or large-scale motions rather than of high temperature. Since the OH could be expected to partake of the velocity of the HII in its immediate vicinity, there would seem to be no reason for expecting it to agree closely with the median velocity in every case. However, the general correspondence of HII velocities indicates that kinematic distances may be inferred as well from the OH velocities alone as from the velocities of the associated HII region. In order to investigate in more detail the OH and HII associations, continuum maps of much higher resolution and greater sensitivity are desirable for a number of the sources.

(iii) *Distribution in Galactic Longitude*

The distribution of OH sources as a function of galactic longitude is now considered. We restrict discussion to the longitude range 255° to 350° and to HII regions with $S_{2700} \geqslant 3$ f.u. The basic results are shown in Table 4, where the l-ranges have been chosen to reflect natural breaks in the intensity of continuum radiation and

spatial density of sources, which in turn are related (though not very precisely) to the spiral arms and their tangential points. A significantly greater fraction of HII regions within 37° of the galactic centre show OH emission. Although we demonstrate below that this effect is quite real, some further analysis is necessary to disentangle selection effects connected with the HII region intensities.

Inspection of the 2700 MHz galactic catalogue shows that the number ratio of weak to intense sources is greater in the region $255° < l < 323°$ than in the region $323° < l < 350°$. This is partly due to the lower overall spatial density of sources which reduces confusion in these regions. In Table 5 we show data as functions of flux density for the two regions $l > 323°$ and $l < 323°$, this division being chosen because the numbers of HII regions and OH sources in each region are statistically significant. Both regions are essentially complete in their listing of HII sources with $S_{2700} \geqslant 7$ f.u., while only for the region $l < 323°$ is the range $3 \leqslant S_{2700} < 7$ f.u. fairly complete.

Table 4. Distribution in galactic longitude of OH sources and HII regions

Longitude range Limits	Extent	Number of HII regions	HII region number density (per degree)	Number of OH sources	Number of HII regions per OH source
255°–276°	21°	10	0·5	0	∞
276°–296°	20°	35	1·75	2	17·5
296°–315°	19°	36	1·9	4	9
315°–323°	8°	22	2·75	1	22
323°–335°	12°	28	2·3	9	3·1
335°–342°	7°	21	3	5	4·2
342°–350°	8°	22	2·75	4	5·5

Table 5. Correlation of OH sources with galactic longitude and HII region intensity

Longitude range	HII region S_{2700} (f.u.)	Number of HII regions	Number of OH sources
255°–323°	$S_{2700} \geqslant 7$	48	4
255°–323°	$3 \leqslant S_{2700} < 7$	55	3
323°–350°	$S_{2700} \geqslant 7$	48	14
323°–350°	$3 \leqslant S_{2700} < 7$	23	4

From a consideration of HII regions with $S_{2700} \geqslant 7$ f.u., the fraction showing OH is more than three times greater for the region $l > 323°$ than for the region $l < 323°$; this difference of a factor of three between the two regions of longitude also applies, but with less significance, to HII regions with $S_{2700} < 7$ f.u.

(iv) *Correlation of OH Emission with HII Region Intensity*

When the number of search positions was increased from 69 (with $S_{2700} \geqslant 11$ f.u.) to 174 (with $S_{2700} \geqslant 3$ f.u.), the total number of detected OH sources increased from 16 to 25, while a search of a further 37 positions with $S_{2700} < 3$ f.u. yielded no new OH sources. This correlation of OH detection with HII region intensity can also be seen from Table 5. Thus, from a consideration of sources with $l < 323°$, we conclude that the fraction showing OH emission is approximately 50% greater for HII regions with $S \geqslant 7$ f.u. than for those with $3 \leqslant S < 7$ f.u. This conclusion is of low significance but also appears to be true of the region $l > 323°$.

In the case of OH emission, the peak flux density of the profile is an adequate representative measure of intensity. In the case of HII regions, the work of Shaver and Goss (1970*b*) demonstrates that the nearby HII region complexes, when observed with high angular resolution, break up into a number of smaller components. When OH is discovered in these sources, it is usually intimately associated with a specific condensation within the complex. Thus, when OH is apparently associated with a distant intense HII region, it is probable that, with higher angular resolution, a much weaker HII condensation within the complex would prove to be associated with the OH. However, since many of the positions of our search have not been observed with high resolution, we have used the HII region flux densities obtained from the Parkes 2700 MHz galactic survey (our initial search list) to compare with the OH intensities.

Since the fraction of HII regions showing OH is smaller for the weaker HII regions, it is of interest to determine whether this arises because the average intensity of the OH associated with the weaker HII regions is lower. However, such an effect is not discernible; the median value of peak flux density is the same for OH associated with the stronger HII regions ($S_{2700} > 7$ f.u.) as for the weaker HII regions ($S_{2700} < 7$ f.u.). Where 'an HII region' really represents a cluster of unresolved HII regions, the stronger sources typically represent a cluster of more HII regions, and so we might expect an increased probability of OH emission.

We conclude that two distinct correlations are present: (1) the probability of detecting OH to a specific sensitivity limit in an HII region of specified intensity is greater for galactic longitudes within about 37° of the galactic centre than for longitudes further from the centre, and (2) the probability of detecting OH to a specific sensitivity limit is lower for weaker HII regions. Neither correlation is as clearly present in OH absorption data. We suggest that both correlations indicate an increase in the conditions conducive to masered OH emission rather than merely to the presence of OH in appreciable densities.

5. Conclusions

The present survey has completed a uniform search for 1665 MHz OH emission from HII regions in the longitude range 255° to 350°. The new sources discovered corroborate earlier conclusions that OH, emitted predominantly at 1665 MHz, is associated with individual HII regions. There are indications that the probability of detecting 1665 MHz OH emission is greater in the direction of more intense HII regions, and is also significantly greater for longitudes nearer the galactic centre (an effect over and above that resulting from the increased density of HII regions in the inner portion of the Galaxy).

The larger sample now available of OH sources associated with HII regions confirms the conclusions (relating to this class of source) which have been derived more tentatively from earlier smaller samples: 1665 MHz emission is generally strongest; 1667 MHz emission is typically somewhat weaker but is present in most instances; 1612 and/or 1720 MHz emission is present occasionally with an intensity comparable with the 1665 MHz emission, but null results for many sources show such accompanying satellite-line emission to be usually at least an order of magnitude weaker than the 1665 MHz emission. In the very strong source OH 330·9−0·4, 1612 MHz emission two orders of magnitude weaker than the 1665 MHz intensity

was detected and satellite-line emission with similarly low relative intensity may be present in many 1665 MHz sources. Prior to the present results, accompaniment of 1665 MHz emission by 1720 MHz emission seemed more prevalent than accompaniment by 1612 MHz emission. However, the occurrence of 1612 MHz emission in three of the present sources now suggests that both occur with approximately equal probability.

The new OH sources show polarization properties and velocity structure similar to those established for earlier small samples. Several narrow features with high degrees of circular polarization are generally present, although simple pairing of features with opposite senses of polarization (expected if Zeeman splitting were the cause of the circular polarization) rarely occurs. Velocities of features observed in different transitions usually show no direct correspondence. The properties are in agreement with the model derived for a few intense sources observed by long-baseline interferometry in which the emission is confined to a small area but arises from a number of independent emitting regions with characteristic radial velocity and sense of polarization. The present discovery of one very intense source and several quite intense ones should allow further long-baseline mapping observations to be made.

References

Beard, M. (1966). *Aust. J. Phys.* **19**, 141.
Beard, M., Thomas, B. MacA., and Day, G. A. (1969). *Aust. J. Phys. astrophys. Suppl.* No. 11, 27.
Caswell, J. L. (1972). *Aust. J. Phys.* **25**, 443.
Caswell, J. L., and Robinson, B. J. (1974). *Aust. J. Phys.* **27**, 597.
Clark, D. H., Caswell, J. L., and Green, Anne J. (1973). *Nature* **246**, 28.
Day, G. A., Caswell, J. L., and Cooke, D. J. (1972). *Aust. J. Phys. astrophys. Suppl.* No. 25, 1.
Day, G. A., Thomas, B. MacA., and Goss, W. M. (1969). *Aust. J. Phys. astrophys. Suppl.* No. 11, 11.
Dickinson, D. F., and Turner, B. E. (1972). *Astrophys. Lett.* **11**, 1.
Ellder, J., Ronnang, B., and Winnberg, A. (1969). *Nature* **222**, 67.
Goss, W. M., Manchester, R. N., and Robinson, B. J. (1970). *Aust. J. Phys.* **23**, 559.
Goss, W. M., and Shaver, P. A. (1970). *Aust. J. Phys. astrophys. Suppl.* No. 14, 1.
Johnston, K. J., Robinson, B. J., Caswell, J. L., and Batchelor, R. A. (1972). *Astrophys. Lett.* **10**, 93.
Manchester, R. N., Robinson, B. J., and Goss, W. M. (1970). *Aust. J. Phys.* **23**, 751.
Milne, D. K. (1970). *Aust. J. Phys.* **23**, 425.
Robinson, B. J., Caswell, J. L., and Goss, W. M. (1971). *Astrophys. Lett.* **9**, 5.
Robinson, B. J., Goss, W. M., and Manchester, R. N. (1970). *Aust. J. Phys.* **23**, 363.
Shaver, P. A., and Goss, W. M. (1970*a*). *Aust. J. Phys. astrophys. Suppl.* No. 14, 77.
Shaver, P. A., and Goss, W. M. (1970*b*). *Aust. J. Phys. astrophys. Suppl.* No. 14, 133.
Thomas, B. MacA., and Day, G. A. (1969*a*). *Aust. J. Phys. astrophys. Suppl.* No. 11, 3.
Thomas, B. MacA., and Day, G. A. (1969*b*). *Aust. J. Phys. astrophys. Suppl.* No. 11, 19.
Turner, B. E. (1970). *Astrophys. Lett.* **6**, 99.
Wilson, T. L., Mezger, P. G., Gardner, F. F., and Milne, D. K. (1970). *Astr. Astrophys.* **6**, 364.
Winnberg, A., Habing, H. J., and Goss, W. M. (1973). *Nature Phys. Sci.* **243**, 78.

Manuscript received 25 February 1974